

Plasma spectroscopy analysis technique based on optimization algorithms and spectral synthesis for arc-welding quality assurance

J. Mirapeix, A. Cobo, D. A. González and J. M. López-Higuera

*Grupo de Ingeniería Fotónica –Universidad de Cantabria
E.T.S.I.I. y Telecomunicación – Dpto. TEISA
Avda. Los Castros s/n – c.p. 39005 Santander, Spain
Tel: + 34-942-200877; Fax: + 34-942-200877
mirapeixjm@unican.es
<http://grupos.unican.es/gif>*

Abstract: A new plasma spectroscopy analysis technique based on the generation of synthetic spectra by means of optimization processes is presented in this paper. The technique has been developed for its application in arc-welding quality assurance. The new approach has been checked through several experimental tests, yielding results in reasonably good agreement with the ones offered by the traditional spectroscopic analysis technique.

©2007 Optical Society of America

OCIS codes: (300.6210) Spectroscopy, atomic; (120.4630) Optical inspection; (000.3860) Mathematical methods in physics

References and links

1. G. Stewart, G. Whitenett, K. Atherton, B. Culshaw, and W. Johnstone, "Optical fibre sensors for environmental monitoring of trace gases," *Proc. SPIE* **4829**, 963-964 (2003).
2. W. B. Grant, R. H. Kagann, and W.A. McClenny, "Optical remote measurement of toxic gases," *J. Air Waste Manage. Assoc.* **42**, 18-30 (1992).
3. R. L. Green, M. D. Mowery, J.A. Good, J. P. Higgins, S. M. Arrivo, K. McColough, A. Mateos, and R. A. Reed, "Comparison of near-infrared and laser-induced breakdown spectroscopy for determination of magnesium stearate in pharmaceutical powders and solid dosage forms," *Appl. Spectrosc.* **59**, 340-347 (2005).
4. S. Acquaviva, E. D'Anna, M. L. De Giorgi, and F. Moro, "Laser-induced breakdown spectroscopy for compositional analysis of multielemental thin films," *Spectrochim. Acta Part B* **61**, 810-816 (2006).
5. B. Andre Weinstock, J. Janni, L. Hagen, and S. Wright "Prediction of oil and oleic acid concentrations in individual corn (*Zea mays* L.) kernels using near-infrared reflectance hyperspectral imaging and multivariate analysis," *Appl. Spectrosc.* **60**, 9-16 (2006).
6. K. C. Lawrence, W. R. Windham, B. Park, D.P. Smith, and G.H. Poole, "Comparison between visible/NIR spectroscopy and hyperspectral imaging for detecting surface contaminants on poultry carcasses," *Proc. SPIE* **5271**, 35-42 (2004).
7. P. B. García-Allende, O. M. Conde, A. M. Cubillas, C. Jaúregui, and J. M. López-Higuera, "New raw material discrimination system based on a spatial optical spectroscopy technique," *Sens. Actuators A* (to be published).
8. C. S. Wu, M. Ushio, and M. Tanaka, "Analysis of the TIG welding arc behaviour," *Comput. Mater. Sci.* **7**, 308-314 (1997).
9. L. Grand, J. Grum, I. Polajnar, and J. M. Slabe, "Feasibility study of acoustic signal for on-line monitoring in short circuit gas metal arc welding," *Int. J. Mach. Tools Manuf.* **45**, 1735-1738 (2005).
10. B. Venkatraman, B. Raj, and M. Menaka, "Online infrared detection of inclusions and lack of penetration during welding," *Mater. Eval.* **63**, 933-937 (2005).
11. G J. Zhang, S. B. Chen, and L. Wu, "Intelligent control of pulsed GTAW with filler metal," *Weld. J.* (Miami, Fla) **84**, 9-16 (2005).
12. P. Sforza and D. de Blasiis, "On-line optical monitoring system for arc welding," *NDT E. Int.* **35**, 37-43 (2002).
13. A. Ancona, V. Spagnolo, P. M. Lugara, and M. Ferrara, "Optical sensor for real-time monitoring of CO₂ laser welding process," *Appl. Opt.* **40**, 6019-6025 (2001).

14. A. Ancona, P. M. Lugara, F. Ottonelli, and I. M. Catalano, "A sensing torch for the on-line monitoring of the gas tungsten arc welding process of steel pipes," *Meas. Sci. Technol.* **15**, 2412-2418 (2004).
15. J. Mirapeix, A. Cobo, O. M. Conde, C. Jaúregui, and J. M. López-Higuera, "Real-time arc welding defect detection technique by means of plasma spectrum optical analysis," *NDT E. Int.* **39**, 356-360 (2006).
16. H. R. Griem, *Principles of Plasma Spectroscopy* (Cambridge University Press, Cambridge, 1997), Chap. 5.
17. W. Lochte-Holtgreven, *Plasma Diagnostics* (North-Holland, Amsterdam, 1968), Chap. 4.
18. A. Marotta, "Determination of axial thermal plasma temperatures without Abel inversion," *J. Phys. D: Appl. Phys.* **27**, 268-272 (1993).
19. J. Mirapeix, A. Cobo, C. Jaúregui, and J. M. López-Higuera, "Fast algorithm for spectral processing with application to on-line welding quality assurance," *Meas. Sci. Technol.* **17**, 2623-2629 (2006).
20. A. B. McLean, C. E. J. Mitchell, and D. M. Swanston, "Implementation of an efficient analytical approximation to the Voigt function for photoemission lineshape analysis," *J. Electron Spectrosc. Relat. Phenom.* **62**, 125-132 (1994).
21. T. Zeh, H. Schweizer, A. Meixner, A. Purde, and A. W. Koch, "Enhancement of detection accuracy of fiber Bragg grating sensors," *Proc. SPIE* **5502**, 540-543 (2004).
22. National Institute for Standards and Technology (NIST) atomic spectra database, http://physics.nist.gov/cgi-bin/AtData/main_asd.
23. W. L. Price, "Global optimization by controlled random search," *Comput. J.* **20**, 367-370 (1977).
24. M. M. Ali, A. Törn, and S. Viitanen, "A numerical comparison of some modified controlled random search algorithms," *J. Global Optim.* **11**, 377-385 (1997).
25. L. O. Vilarinho and A. Scotti, "Proposal for a modified Fowler-Milne method to determine the temperature profile in TIG welding at low currents," *J. Braz. Soc. Mech. Sci. Eng.* **26**, 34-39 (2004).
26. I. B. Gornushkin, A. Ya. Kazakov, N. Omenetto, B. W. Smith and J. D. Winefordner, "Experimental verification of a radiative model of laser-induced plasma expanding into vacuum," *Spectrochim. Acta Part B* **60**, 215-230 (2005).
27. A. Cobo, "Contribución al desarrollo de sistemas sensores para monitorizado y medida de vibraciones basados en tallos de fibra óptica," (PhD Thesis, Universidad de Cantabria, 1998), Chap. 7.

1. Introduction

There is a great variety of optical spectroscopic techniques covering a large range of different application scenarios. From the use of absorption spectroscopy for environmental monitoring in different spectral bands [1, 2], to pharmaceutical research [3], applications focused on art and archeology, or the analysis of compounds [4], spectroscopic approaches offer rich information about the processes or materials under analysis. The study of the information contained in the spectra, analyzing particular emission or absorption lines, relations between several spectral peaks or even the background radiation, is commonly an efficient approach when an optical solution is feasible.

A relevant niche for optical spectroscopic techniques is the inspection of different industrial processes, typically regarding quality assurance. Examples can be found in the processing of food [5, 6], tobacco [7] and the manufacturing of electronic devices. Some promising solutions have also been developed for on-line quality assurance of arc and laser-welding processes. The complexity of the physics involved in these processes has made it difficult to formulate a generic theoretical model able to relate efficiently all the parameters involved [8]. This lack of a mathematical framework has led to basing welding quality assurance on procedure trials where the optimal input welding parameters are determined and off-line destructive and non-destructive evaluation techniques, like penetrant liquids, X-rays, ultrasonics, magnetic particles or macrographs. These solutions are usually expensive in productivity terms. Thus, the search for an efficient on-line welding quality monitoring system, able to early detect defects in the welds, has become an active area of research. The introduction of arc and laser welding processes in some relevant industrial areas, like aeronautics or nuclear, where quality assurance plays a major role, has also contributed to this research effort.

Regarding arc-welding, several on-line monitoring techniques have been proposed, from the analysis of the plasma acoustic emission [9] to the use of infrared thermography [10] or machine-vision [11]. Plasma emission spectroscopy seems also promising, due to the correlation between some spectroscopic variables, like the plasma electronic temperature T_e , and the resulting weld quality [12, 13]. Its use exhibits several key advantages, like the

possibility of a non-invasive arrangement of the input optics, the electromagnetic immunity of optical fiber sensors and the possibility of performing different analyses with the various chemical species participating in the plasma.

The feasibility of a real-time, on-line implementation of spectroscopic-based solutions has been demonstrated [14, 15]. However, there are still some difficulties in unambiguously interpreting the T_e profiles, especially when trying to identify different kinds of weld defects. In this sense, an erroneous selection of the atomic emission lines contributing to the determination of T_e can lead to both false alarms and undetected defects. Hence, an alternative technique to verify the results obtained with the traditional spectroscopic approach would be useful. In this paper, a new spectroscopic analysis technique originally designed for the analysis of the arc-welding process is presented. The use of optimization algorithms and the generation of synthetic spectra permit the determination of the participation percentage of some key atomic species within the plasma. The resulting profiles show a direct correlation with the resulting weld quality, making them an alternative technique for performing quality analyses of arc-welding processes. TIG-welding tests will show the feasibility of the proposed technique, validating its results with the traditional T_e profiles.

2. Plasma spectroscopy

A typical plasma spectrum is composed of several atomic emission lines, corresponding to transitions of neutral atoms or ions of those atomic species contributing to the plasma. Usually a significant background radiation appears, commonly referred to as *Bremmstrahlung* [16]. The spectroscopic analysis in the particular case of the welding quality assurance problem lies mainly in the determination of the plasma electronic temperature T_e . As mentioned in Section 1, it is known that the profiles of this parameter present a correlation with the quality of their associated seams [12, 13]. Although there are different ways to obtain an estimation of T_e [17], it is typically computed using the following simplification, which involves only two different emission lines in the calculation

$$T_e = \frac{E_m(2) - E_m(1)}{k \ln \left[\frac{I(1)A(2)g_m(2)\lambda(1)}{I(2)A(1)g_m(1)\lambda(2)} \right]}, \quad (1)$$

where E_m is the upper level energy, I the emission line intensity, A the transition probability, g_m the statistical weight and λ the wavelength of emission lines (1) and (2), which have to be from the same element in the same ionization stage. A more stable estimation of the plasma temperature can be obtained by means of the so-called *Boltzmann-plot*, where several different emission lines of the same element can be considered.

$$\ln \left(\frac{I_{mn}\lambda_{mn}}{A_{mn}g_m} \right) = \ln \left(\frac{hcN}{Z} \right) - \frac{E_m}{kT_e}. \quad (2)$$

In Eq. (2) h is the Planck's constant, c the light velocity, N the population density of the state m , Z the partition function, k the Boltzmann constant and n the other state contributing to the transition. When the left hand side of Eq. (2) is plotted against the excitation energies, the slope of the resulting graph is inversely proportional to T_e . Equation (2) is derived from the *Boltzmann equation*

$$N_m = \frac{N}{Z} g_m \exp \left(\frac{-E_m}{kT_e} \right). \quad (3)$$

The expression relating the intensity of an emission line induced by a transition from the level m to n to the population density of the upper level N_m is

$$I_{mn} = N_m A_{mn} h \gamma_{mn}, \quad (4)$$

where γ_{mn} is the frequency associated with the emission line. Equation (4) is valid for optically thin plasmas, condition that is commonly accepted for arc-welding plasmas [14, 18].

Despite the higher reliability of the plasma temperatures obtained with Eq. (2), the simplified Eq. (1) is commonly employed in on-line monitoring applications due to its lesser computational cost. It is worth noting that the separation between the upper level energies E_m associated with the selected emission lines has to be maximized to obtain an accurate T_e estimation. This separation can be derived from Eq. (5), which determines the uncertainty in the computation of the temperature

$$\frac{\Delta T}{T} = \frac{kT}{E_m(1) - E_m(2)} \frac{\Delta(I(1)/I(2))}{I(1)/I(2)}. \quad (5)$$

In Eq. (5), $\Delta T/T$ is the temperature uncertainty and $\Delta I(1)/I(1)$ the uncertainty in the transition probability of the selected emission line.

3. Proposed spectroscopic analysis technique

Several processing stages have to be considered for the on-line estimation of T_e . A schematic description of the system proposed in a previous paper is depicted in Fig. 1 [19].

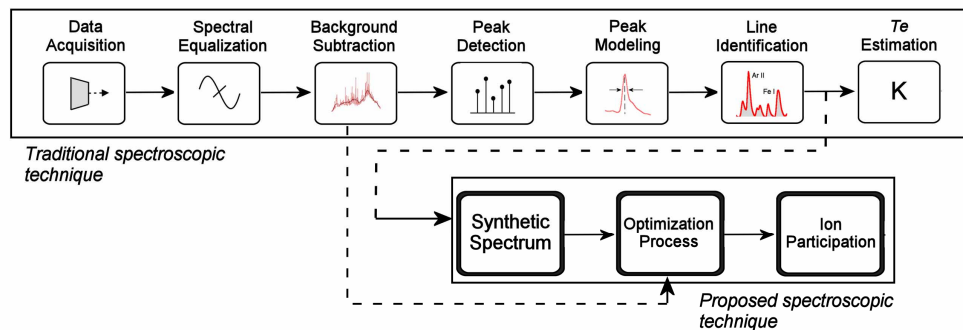


Fig. 1. Processing schemes of traditional and proposed spectroscopic analysis techniques

Plasma radiation (generated during the arc-welding process) is captured by means of an optical sensor system. The spectral response of the whole input optical system (e.g. optical fiber, spectrometer) has to be considered to avoid spectral distortion of the collected data. As mentioned above, the plasma spectra usually present a significant background radiation, which is removed by means of a smoothing algorithm. Some of the multiple emission lines must be selected establishing a signal-to-noise rejecting threshold. These lines are modeled using a simplified Voigt function [20] and a sub-pixel algorithm to accurately estimate the peak central wavelength [21]. This parameter is especially relevant for identifying the emission lines. A local copy of a NIST database [22] is used to associate each emission line with its corresponding chemical species and ionization stage. The identification stage is somewhat important, as incorrect identifications will produce erroneous T_e estimations when using Eq. (1) or Eq. (2). The emission lines selected for the analysis have to be free from self-absorption, and an estimation of the temperature uncertainty obtained with them must be also carried out [19]. Finally, as stated in Section 1, a correlation will be established between the resulting T_e profiles and their associated welds.

The proposed technique makes use of these processing stages with the exception of the T_e estimation. Once the significant emission lines have been selected, some of them, following a criterion of number of appearances in the different spectral captures, will contribute to the generation of the *synthetic* spectrum. Only emission lines with known relative intensities in

the NIST database are used in the synthetic spectra and, therefore, in the optimization process, as these relative intensities are employed to generate the synthetic spectrum of each ion and neutral atom considered. The species likely to appear in this process will be those included in the material to be welded and the welding shielding gases. The optimization process starts after the ions and neutral atoms contributing to the synthetic spectrum have been selected.

Controlled Random Search (CRS) optimization algorithms [23] have been chosen for this stage considering that their characteristics are suitable for the spectral minimization problem. For each spectral capture, the function to minimize (fitness function) will be the mean square error between the real welding spectrum and the synthetic one, evaluated in all the emission lines contributing to each ion or neutral atom synthetic spectrum. Considering that the dimension of the optimization problem will be the number of ions and neutral atoms contributing to the synthetic spectrum, the variation of their participation percentage will allow to gradually reduce the error arising from the computation of the fitness function, until a given stopping condition is satisfied or the number of global and local iterations is exceeded. Participation can be here defined as the relative concentration of the species (neutral atoms and ions) participating in the plasma [proportional to N in Eq. (2)]. The repetition of the above process with all the spectral captures associated with a particular welding process gives rise to detailed profiles indicating the participation percentage of the relevant neutral atoms and ions in the plasma. CRS algorithms are introduced in the following Section.

4. Controlled random search optimization algorithms

When a particular problem is described in terms of a cost function that has to be minimized, the process of looking for the optimal solutions can be extremely complex. A good example of the so-called optimization process is the search for the optimal route for a logistics business, trying to minimize both time and fuel costs. Multiple variables may be necessary to model the problem under analysis, several different solutions can be valid, and the computational cost tends to be high. Optimization algorithms have evolved and they can be classified into several groups depending on the search technique employed. A classification example can be established by dividing the optimization methods between those which only need evaluations of the function to be minimized, and those which also required evaluations of the derivative of that function.

A mathematical formulation of a generic optimization problem can be expressed in the following terms

$$f : S \subset \mathbb{R}^n \rightarrow \mathbb{R} \quad (5)$$

$$\text{find } x^* \mid f^* = f(x^*) \leq f(x) \quad \forall x \in S .$$

where S is the search space, $f(x)$ is the function to minimize, and f^* the minimum. In practical problems, an approximation of x^* will be enough, satisfying a criterion so that

$$\left| f^* - f(\hat{x}^*) \right| \leq \varepsilon , \quad (6)$$

where \hat{x}^* is the approximation and ε the error assumed in that approximation, also called the *stopping condition*.

Controlled Random Search (CRS) algorithms were initially developed for processes involving non-analytical cost functions. They can be described as a *direct search* technique, and are purely heuristic. Basically, an initial set of N points is chosen and then iteratively contracted by substituting the worst point with a better one. CRS algorithms evolved from simple random search methods, where only the best point was retained in each iteration. In CRS algorithms, the replacement point can be determined by means of a global technique, but a local one can also be introduced to search in a smaller region. An efficient implementation of these CRS algorithms is CRS6 [24], which can be summarized as follows:

1. N points within the search space must be randomly selected and evaluated.

2. The best points according to the evaluation of the fitness function are selected and two more are randomly selected from the point set. A multi-dimensional parabolic interpolation is performed with these three points, evaluating the interpolation maximum. If a worst point is obtained, or the established limits are exceeded, then step 2 must be repeated. If the point is found to be the best one, then it has to be substituted and step 4 has to be processed.
3. Finish if the stopping condition is fulfilled.
4. "Local phase": to be repeated M times each time, or finish if the stopping condition is satisfied. A new random point is selected, using a beta-probability distribution, whose mean will be the best point coordinates, and with a standard deviation obtained from the distance between the best and worst points. The new point has to be evaluated and, if it is a best new one it has to be substituted.

In the following Section experimental results are provided showing that the participation profiles obtained using CRS algorithms within the proposed spectroscopic analysis technique show a clear correlation with the welding quality of their associated seams.

5. Experimental issues

The validation of the proposed technique was carried out by performing several arc-welding tests within the laboratory. A Tungsten Inert Gas (TIG) welding system, which is schematically depicted in Fig. 2, was used to generate seams in AISI-304 stainless steel plates.

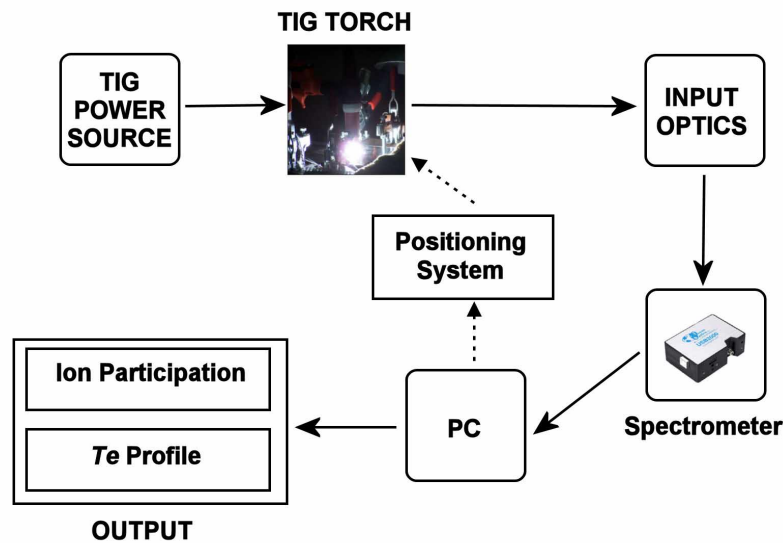


Fig. 2. TIG welding quality assurance system scheme.

The welding system is formed by a Kemppi Mastertig 2200 power source and a TIG torch attached to it. The tungsten electrode (1 mm diameter) with a conical tip preparation was placed at approximately 2 mm from the plates during the welding tests. Argon was employed as shielding gas, with an initial flow rate of 12 L/min. A positioning system, formed by a controller (Newport MM4005) and two linear stages (Newport MTM100PP1) with 1 μ m resolution, was controlled by means of a PC to generate the desired weld trajectories. Two different alternatives were used as input optics of the spectroscopic system. A configuration based on a collimator (7 mm diameter) attached to an optical fiber (Ocean Optics P400-UV-

VIS) was used, as well as an optical fiber (Ocean Optics P50-UV-VIS) embedded within the TIG torch, guiding the fiber tip through one of the gas nozzle exits. Both configurations are schematically depicted in Figs. 3(a) and 3(b) respectively.

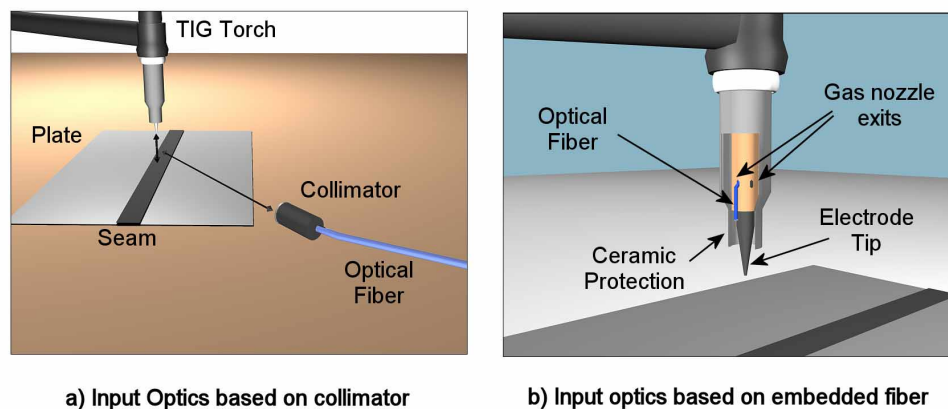


Fig. 3. Scheme of input optics configurations.

It is worth noting that, in terms of the processing scheme presented in Fig. 1, the use of different input optics configurations does not affect the result of the spectroscopic analysis, as the spectral response of both options is considered in the spectral equalization processing stage. In the two cases mentioned above, the plasma radiation is delivered to a CCD spectrometer (Ocean Optics USB2000), with 2048 pixels, a spectral resolution of 0.3 nm and a spectral range from 195 to 535 nm. The whole system, including the TIG power source, the spectrometer and the positioning system, is controlled by a conventional desktop PC, which also performs the processing tasks. The tests performed regarding the proposed spectroscopic analysis technique were run on a dual-core 3 GHz processor desktop PC with 2 GB of RAM. The code was implemented in the C# programming language.

Several tests were performed to check the results delivered by the new technique. As an initial study of the performance of the CRS6 algorithm, a single plasma spectrum obtained during a TIG welding test was replicated to generate a set of 150 identical spectral captures. In this way, the ability of the optimization algorithm to converge to the same expected result can be checked in terms of parameters such as the stopping condition ϵ or the maximum number of iterations. The spectrum used to create the set of spectral captures is shown in Fig. 4. It can be seen that, as mentioned in Section 3, the plasma spectrum exhibits a significant background radiation, as well as several atomic emission lines.

Table 1 contains the data of the different simulations performed with CRS6, where *condition* is the CRS6 stopping condition ϵ , *participation* is the relative concentration (%) of neutral atoms and ions participating in the plasma, *std* is the standard deviation, and *error* is the CRS6 optimization error, computed as the mean square error between the real plasma spectrum and the synthetic one. *Global* and *local iterations* are the number of iterations performed during the optimization process in the global and local search techniques, and *processing time* is the estimated computational time of the optimization process. Ar I and Ar II were selected as indicators of the stability of the results offered by the algorithm for different captures. The mean value of the neutral atom and ion participations, and also the mean standard deviation of the whole process, considering the 150 spectral captures, are shown. The standard deviation of the participation percentage is a good indicator of the ability of CRS6 to converge to the same solutions for all the considered captures. As expected, the Ar I and Ar II participation profiles are less noisy for more demanding ϵ . Another indicator of the performance of CRS6 is the error of the optimization process itself. It can be seen that, for ϵ

less than 1, the error remains within the same range (in fact it diminishes, but considering more decimal positions). Precisely for that range of ε , the mean standard deviation for both Ar I and Ar II is less than 1. This reduction in the overall process error is a result of the increased number of the iterations of the both global and local search techniques required for smaller ε . The processing time also increases accordingly to the total number of iterations required for the optimization process.

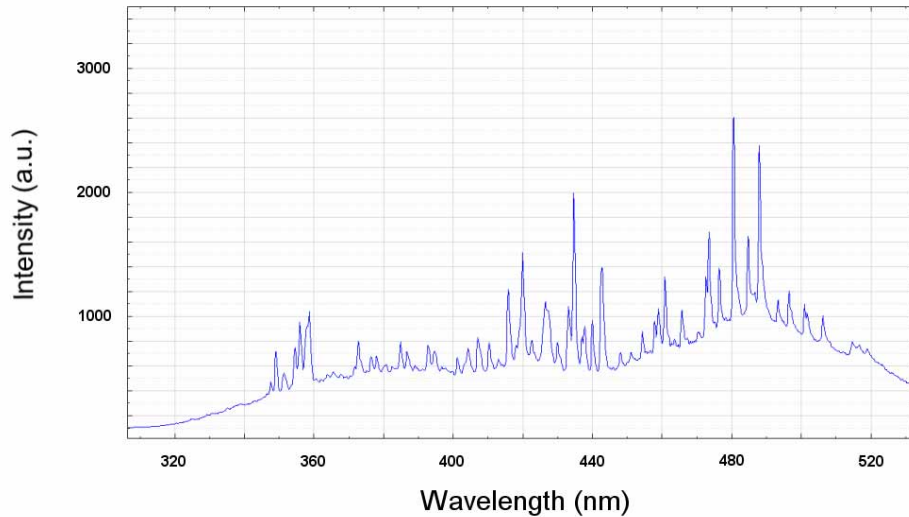


Fig. 4. TIG welding plasma spectrum.

An example of the optimization process for the plasma spectrum shown in Fig. 4 is depicted in Fig. 5. The real plasma spectrum (blue) is presented after the line identification stage (see Fig. 1). Some lines have been identified as Ar II or Cr I, while others remain unclassified. The synthetic spectrum (red) is formed by the contribution of all the neutral atoms and ions considered. The synthetic spectrum exhibits peaks for all the identified emission lines. Some line intensities of the synthetic spectrum tend to be close to the real ones, while some discrepancies appear in lines like the one identified as Cr I at approximately 476 nm. Incorrect line identifications and the use of the line relative intensities provided by the NIST local database for the generation process of the synthetic spectrum over a wide spectral range could be the cause of these discrepancies. Although an improvement in the match between real and synthetic spectra will be studied in future works (some possible solutions in this regard will be discussed in Section 6), the following experimental tests show that the proposed analysis technique is feasible for weld defect identification.

Table 1. Performance of CRS6 for different stopping conditions

Condition (%)	Ar II (% participation)		Ar I (% participation)		Global Iterations	Local Iterations	Error	Processing Time (s)
	Mean	Std	Mean	Std	Mean	Mean	Mean	Mean
50	16.42	7.33	19.21	9.33	519	17	0.126	0.11
10	19.91	2.11	13.33	3.43	1156	113	0.067	0.23
5	20.75	1.78	13.18	1.93	1326	157	0.063	0.27
1	22.12	0.66	13.56	0.83	1600	243	0.061	0.34
0.5	22.27	0.51	13.59	0.87	1740	268	0.061	0.37
0.1	22.51	0.50	13.89	0.35	2049	363	0.061	0.44
0.05	22.69	0.46	13.97	0.16	2211	410	0.061	0.48
0.01	22.95	0.22	13.99	0.08	2547	534	0.061	0.57
0.001	23	0	13.99	0.08	3008	710	0.061	0.69
0.0001	23	0	14	0	3341	891	0.061	0.79

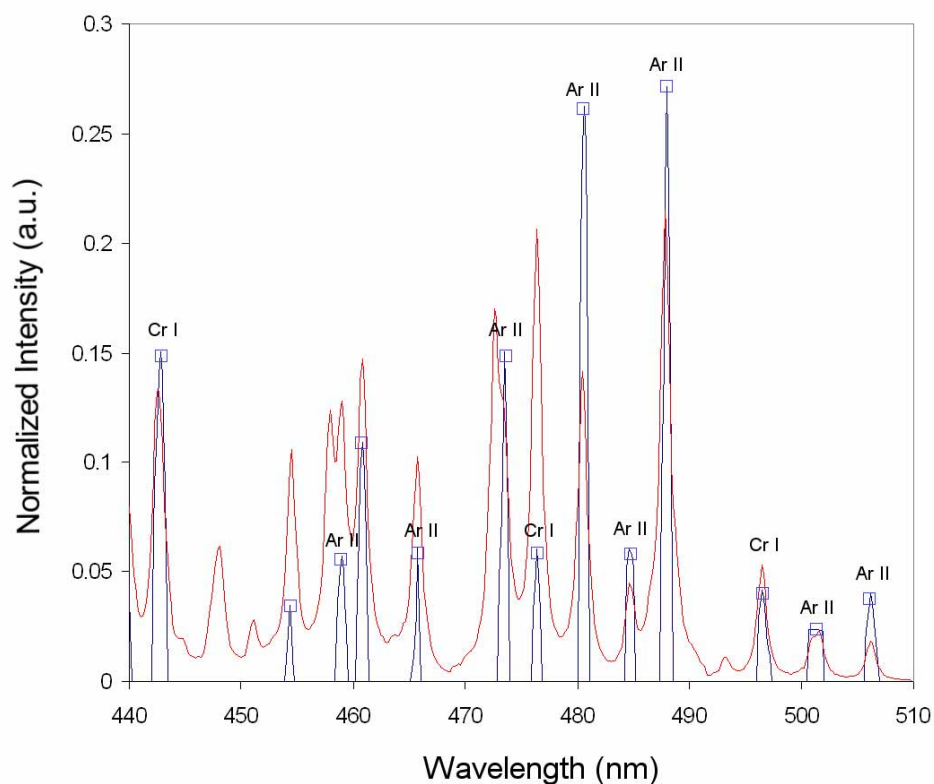


Fig. 5. Example of optimization process: real plasma spectrum (blue) after emission line identification and synthetic spectrum (red).

Several tests have been carried out considering real welding plasma spectra, with $\varepsilon = 0.001$ in all of them. An example is presented in Fig. 6, where a weld seam was performed using two

different welding currents of 42 and 37 A alternatively. In Fig. 6(a) the resulting seam is presented, where slight variations produced by the current variations in the seam width can be observed. The participation percentage of Ar I, Ar II and Cr I are depicted in Fig. 6(b). The welding current is also included in Fig. 6. The Ar II participation profile exhibits a clear correlation with the welding current variations, and hence with the slight variations in the seam width. The profile associated with Ar I shows the same correlation with the welding current at the beginning of the process, but this relation becomes more diffuse at the end of the process. The Cr I profile has also some correlation with the welding current, but in this case the resulting signal is noisier.

An interesting result is presented in Fig. 7. In this case the weld was performed with a constant welding current of 40 A. A small defect in the seam was provoked at $x \approx 5$ cm, where the shielding gas flux was reduced from 12 L/min to 6 L/min during approximately 0.5 s. Figure 7(a) presents the resulting seam with the discontinuity at $x \approx 5$ cm. The T_e profile associated with this weld was calculated by using Eq. (2) with several Ar II emission lines. A clear perturbation can be seen in Fig. 7(b) in the T_e profile at the location of the defect. The results obtained with the proposed technique are displayed in Fig. 7(c), including the participation profiles of Ar II, Fe I and Mn I. There is a clear correlation between the T_e profile and the Fe I and Mn I profiles. The profile corresponding to Ar II presents a subtle variation at the location of the defect, but in this case the correlation with the T_e profile is not so clear.

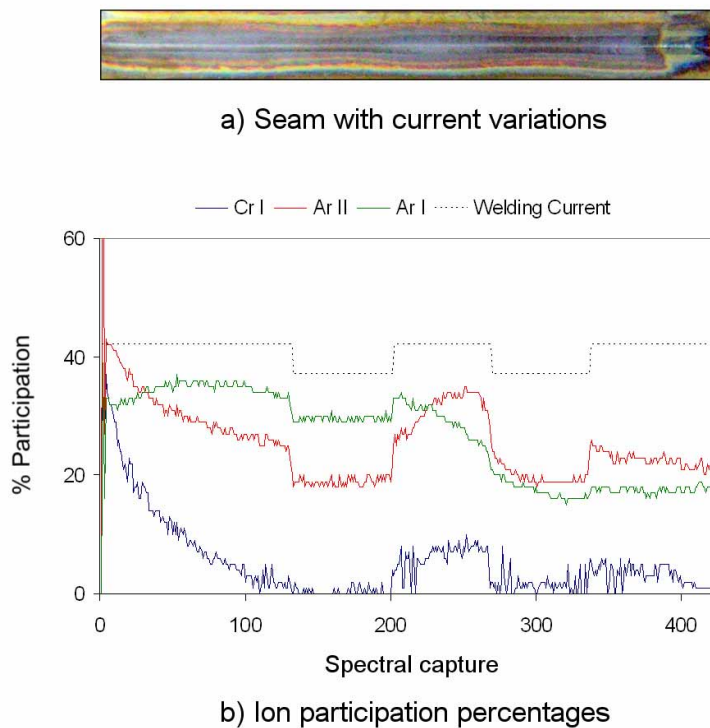


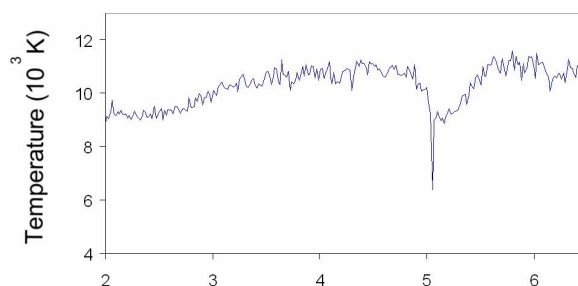
Fig. 6. Detection of seam width variations by means of ion participation profiles.

A similar example is presented in Fig. 8. Figure 8(a) shows the bottom of a seam with two small discontinuities. The T_e profile shown in Fig. 8(b), again determined by means of Eq. (2)

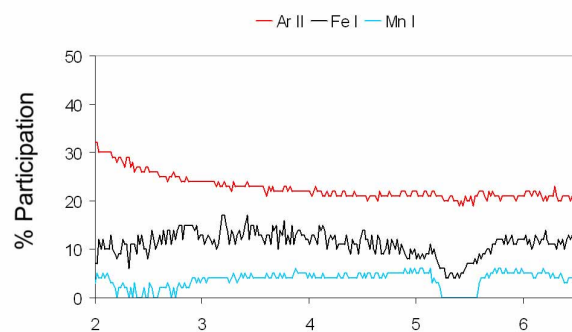
and several Ar II lines, has two clear perturbations at the locations of both defects ($x \approx 4.5$ and $x \approx 6.5$ cm). The identification of the defect at $x \approx 4.5$ cm is due to an erroneous identification of an emission line when using CDA as sub-pixel operator [18]. The use of other sub-pixel algorithms to estimate the central wavelength of the emission lines involved in the calculations do not allow to identify that defect. The participation profiles of Ar II, Ar I and Mn I are presented in Fig. 8(c). In this case the Ar II profile does not provide any clear correlation with the quality of the weld [Fig. 8(a)]. The profile associated with Ar I exhibits some subtle perturbations at the defect locations. The Mn I profile is not as stable as the Ar I and Ar II ones, but the perturbations associated with both defects are stronger.



a) Seam with defect



b) Plasma T_e profile

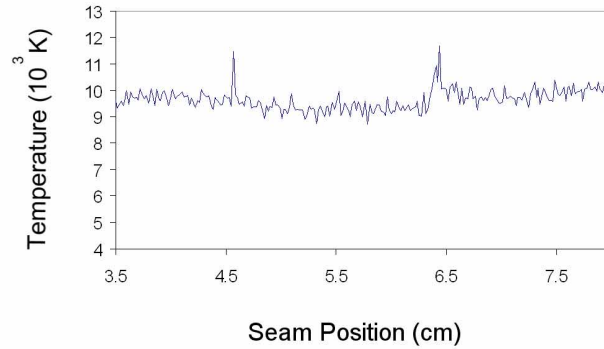


c) Plasma ion participation profiles

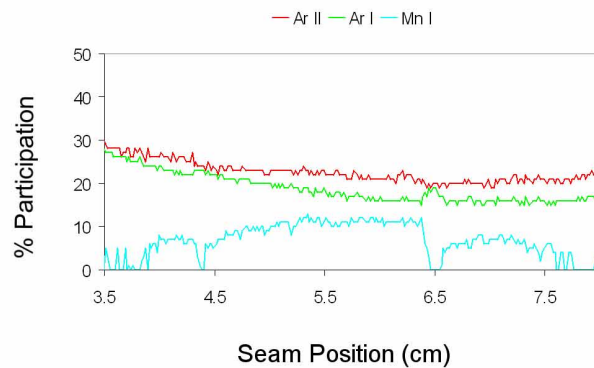
Fig. 7. Comparison of traditional and proposed techniques: identification of seam discontinuity.



a) Seam with defects



b) Plasma T_e profile



c) Plasma ion participation profiles

Fig. 8. Comparison of traditional and proposed techniques: identification of subtle seam defects.

The perturbations associated with the participation profiles depicted in Figs. 7 and 8 are summarized in Table 2. In both cases it can be seen that the perturbations in the participation profiles (measured as the standard deviation (*std*) of those signals), exceed the one calculated for the plasma temperature T_e . Both studies were performed for a section free of defects in the weld seam, particularly from $x = 3$ to $x = 4.8$ cm in the case of weld test no. 1 (Fig. 7) and $x = 4.7$ to $x = 6.2$ cm for weld test no. 2 (Fig. 8). An improvement in the stability of the participation profiles would be desirable for an on-line control of the welding process.

Table 2. Stability of the participation profiles

Weld test no. 1 (Fig. 7)							
Ar II (% participation)		Fe I (% participation)		Mn I (% participation)		Plasma temperature (10^3 K)	
Mean	Std	Mean	Std	Mean	Std	Mean	Std
22.08	1.01	12.11	2.01	4.42	0.61	10.64	0.32

Weld test no. 2 (Fig. 8)							
Ar II (% participation)		Ar I (% participation)		Mn I (% participation)		Plasma temperature (10^3 K)	
Mean	Std	Mean	Std	Mean	Std	Mean	Std
22.28	0.89	18.23	1.71	10.53	1.19	9.33	0.24

6. Conclusion

A new spectroscopic analysis technique based on the use of optimization algorithms to determine the participation profiles of plasma ions and neutral atoms has been proposed. It has been checked by means of several TIG welding tests, showing correlation between the ion and neutral atom participation profiles and the quality of their associated weld seams. Results considering the traditional approach of determining the plasma T_e profiles have also been included as an additional validation of the proposed technique. Although with promising results, several issues remain to be addressed which could improve the performance of the proposed technique.

Regarding the determination of the neutral atom and ion participation profiles of a given species, it is remarkable that they are independently computed during the optimization process. This could lead to an incorrect partitioning between ionization stages. The inclusion of the Saha Equation in the process should be considered, as it allows to determine the ratio of the densities of two consecutive ionization stages of a given species [16, 17], yielding a more realistic estimation of the partitioning.

The generation of synthetic spectra could also be revised. In the proposed technique the synthetic emission line intensities are obtained from a NIST local database. However, the use of those relative intensities over a wide spectral range may cause discrepancies found in the optimization process in specific emission lines. This could be the origin of the lack of response associated with defects observed in the Ar II profiles, as the lines associated with Ar II predominate in the spectral range analyzed [25]. Using the T_e estimation to obtain the desired emission line relative intensities might be a better alternative. Although based in a more sophisticated theoretical model, a similar approach is used in [26] in terms of the need for an initial temperature estimation (and the number densities of the species involved) to produce synthetic spectra. A Monte Carlo optimization is used in this case for the validation of a radiative model of laser-induced plasma.

Different alternatives for the optimization process can be considered. It is worth noting that variations of the CRS6 algorithm [27] and genetic algorithms have already been checked, with similar results to the ones obtained with CRS6 in terms of participation profiles, but with higher computational cost. Although an implementation of the proposed technique as an on-line quality assurance system is feasible, questions regarding the reduction of both processing times and noise in the participation profiles remain to be addressed. Tests involving arc-welding processes in real industrial scenarios are currently being performed.

Acknowledgments

The authors thank the Spanish Government's Ministry of Science and Technology for its support via the TEC'2004-05936-C02-02 and TEC'2005-08218-C02-02 projects. They also thank D. Encinas and J.J. Valdiande for their valuable help.